Dalton Transactions

Accepted Manuscript

ROYAL SOCIETY OF CHEMISTRY

www.rsc.org/dalton

Cite this: DOI: 10.1039/c0xx00000x

www.rsc.org/xxxxxx

ARTICLE TYPE

Structural studies of copper(II) complexes with 2-(2-aminoethyl)pyridine derived Schiff bases and application as precursors of thin organic-inorganic layers

Magdalena Barwiolek[a]*, Edward Szlyk[a], Andrzej Berg[a], Andrzej Wojtczak[a], Tadeusz Muziol[a], Julia Jezierska[b]

Received (in XXX, XXX) Xth XXXXXXXXX 200X, Accepted Xth XXXXXXXXX 200X
DOI: 10.1039/b000000x

Cu(II) complexes with Schiff bases derived from 2-pyridin-2-ylethanamine were obtained and characterized by UV-VIS, fluorescence, and IR spectra. The X-ray crystal structures determined for [Cu(II)(epy(di-*t*-Buba))Cl]x0.042H_2O and [Cu(II)(epy(di-*t*-Buba))O_2CCH_3] revealed tetrahedral distortion of Cu(II) coordination sphere in the solid phase. For both molecules the Cu(II) ions were found in tetragonal environments, what was confirmed by the values of EPR g-matrix diagonal components. The thermal properties of the complexes and gas phase composition were studied by TG/IR techniques. Thin layers of studied copper(II) complexes were deposited on Si(111) by a spin coating method and characterized with a scanning electron microscopy (SEM/EDS), atomic force microscopy (AFM) and fluorescence spectra. For copper(II) layers the most intensive fluorescence band from intra-ligand transition was observed between 498 and 588 nm. The layers fluorescence intensity was related to the rotation speed and deposition time.

Introduction

Study of copper(II) complexes with Schiff-base ligands has become a point of interest for their intriguing structural features, and potential application in various fields. These compounds are known for their biological role and fluorescence properties. Schiff base derivatives incorporating a fluorescent moiety are useful tool for optical sensing of metal ions.[1] Synthesis of Schiff bases and their complexes as the fluorescent materials have also received an extensive concern.[2]

Pyridine ligands have been used in coordination chemistry for variety of metals[3-7] and it has been stated that they play unique role in synthesis of the biologically active compounds.[8] The fluorescence properties and interaction with DNA of the Schiff bases obtained from imidazole derivatives (*N*-((1*H*-imidazole-2-yl)methyl)-2-(pyridine-2-yl)ethanamine, *N*-((1-methyl-1*H*-imidazole-2-yl)methyl)-2-(pyridine-2-yl)ethanamine; 2-(pyridine-2-yl)-*N*-((pyridine-2-yl)methyl)ethanamine) and their copper(II) complexes were studied as well.[9] It has been stated that these complexes effectively interact with CT-DNA through groove binding mode, resulting in strong conformational changes of the CT-DNA. Copper(II) complexes with imine ligands containing imidazolate bridging groups (eg *N*,*N*'-bis(2-substituted-imidazol-4-ylmethylidene)-1,4-diaminobutane) have been used as precursors of highly ordered structures.[10-12] Imidazole and oxadiazole-type materials have been used as ETMs in the blue fluorescent OLEDs.[13] As a result, highly efficient amplified spontaneous emission as well as blue and white organic light-emitting diodes (OLEDs) were demonstrated with these imidazole derivatives. As a result, highly efficient amplified spontaneous emission as well as blue and white organic light-emitting diodes (OLEDs) could be demonstrated with these imidazole derivatives.[14] Thin organic and organometallics films have attracted a research interest due to their technologically important optical and electronic properties.[15] These materials exhibit luminescence, they are used as conductors, semi-conductors, organic light emitting diodes (OLED) and drug transporters.[16-17] Also many thin films of metal complexes, such as Zn(II), Pt(II), Cu(II) or Ag(I) with Schiff bases (e.g. *N*,*N*'-bis(salicylidene)-1,2-ethylenediamine, bis(2-(2-hydroxyphenyl)benzothiazole) were synthesised and their luminescence properties have been employed in organic optoelectronics.[18-22] Some of those films were spin coated or vacuum deposited (4,4'-bis(9-carbazolyl)biphenyl and 2(4-biphenyl)-5-(4-tert-butylphenyl)-1,3,4-oxadiazole.[23] However, there are only few reports on copper(II) compound materials. Some of them were obtained by laser ablation, catodoluminescence or by spin coating.[13, 24-27]

The optical and structural properties of the thin copper(II) layers were also studied. In the case of CuPc (Pc- tetra tricarbethoxyethyl substituted phthalocyanine), the absorption increase was noted at higher copper concentration in the layers.[24] The thin layers of the copper(II) complexes $[Cu_3(opba)(pmdta)_2](NO_3)_2$ (pmdta=1,1,4,7,7-pentamethyl-diethylenetriamine, opba=orthophenylenebis(oxamato) on SiO_2/Si by spin coating technique were obtained. The materials exhibited results pointed out the spin coating is promising method for thin layers of transition metal complexes deposition. The obtained films were thin and homogenous with small crystalities on the surface.[13] Also spin coating technique was used for $[nBu_3P)_3Cu\text{-}O_2CCH_2CO_2\text{-}Cu(PnBu_3)_3]$ and $[(nBu_3P)_3Cu\text{-}O_2C(CH_2)_2CO_2\text{-}Cu(PnBu_3)_3]$ on SiO_2/TiN/Cu deposition. The obatined layers were than heated up to 450°C, resulting in the complexes layers to CuO decomposition. The CuO layers exhibited some cracks.[28] SEM results of this films showed not completely homogeneous layers and defects. This was explained by the different film thickness obtained during the spincoating process, which upon heating produced defects due to unequal evaporation leading to partially cracked copper films. However, this results indicated that spin coating technique could be used instead of CVD method for non volatile compounds to get thin metallic materials.

Previously, copper(II) and nickel(II) complexes with optically active Schiff bases derived from (1*R*,2*R*)(-)cyclohexanediamine were deposited by us on silicon or glass using the spin coating method.[29-30] The obtained materials exhibited luminescence, which depends on the spin coating parameters and structure of complex.

The facts mentioned above: the fluorescence properties of the pyridine derivatives and their complexes, the possibility of using the spin coating technique to deposition of the copper(II) complexes on different substrates and likely fluorescence behaviour of the obtained layers prompted as to synthesize a series of copper(II) complexes with new Schiff bases derived from 2-(2-aminoethyl)pyridine and several aldehydes. These complexes were characterized by X-ray crystallographic, spectroscopically, their fluorescence properties were also studied. The new copper(II) complexes were used as precursors of thin layers in spin coating technique. Morphology of layers were analyzed by AFM and SEM microscopy; and the fluorescence properties of the layers were also studied.

Experimental

Materials

2-pyridin-2-ylethanamine (epy) (95%), 3,5-ditert-butyl-4-hydroxybenzaldehyde (di-*t*-Buba) (99%), pyridine-2-carbaldehyde (pyca) (99%), 1H-imidazole-5-carbaldehyde (4Him) (98%), pentane-2,4-dione (acacH) (97%) were purchased from Aldrich. Copper(II) chloride dihydrate and copper(II) acetate hydrate (analytical grade) were supplied by POCH (Gliwice Poland) and used as received.

Methods and instrumentation

UV-Vis absorption spectra were recorded on a Milton Roy Spectronic 1201 in CH_3CN (1 x 10^{-5} M) solution and with a Specord M-40 (Carl Zeiss Jena) spectrophotometer as Nujol mulls. IR spectral experiments were performed on a Spectrum 2000 Perkin/Elmer FT IR using KBr discs in the range 400-4000 cm^{-1} and PE discs in the range 400-70 cm^{-1}. ^1H, ^{13}C, ^{15}N NMR of ligand spectra were collected with a Bruker 400 MHz in $CDCl_3$, against TMS standard. Elemental analysis of C, H, N were performed on a Vario Macro CHN analyser (Elementar Analysensysteme GmbH), whereas copper elemental analysis was carried by Atomic Absorption Spectroscopy (AAS) as Cu^{2+} salt on atomic absorption spectrometer (Carl Zeiss-Jena). Thermal analysis (TG, DTG, DTA) was performed on a SDT 2960 TA analyzer at nitrogen flow (60 ml/min), heating rate 5°C/min and heating range up to 1200 °C. Gaseous products of thermal decomposition were detected by a FT IR Bio–Rad Excalibur spectrophotometer equipped with a thermal connector heated to 200 °C for gases evolved from a SDT 2960 TA analyser. Powder X-ray diffraction data for the thermal analysis residues were obtained with a Philips X'PERT diffractometer using Cu Kα radiation.

The EPR spectra were measured using a Bruker ELEXYS E500 spectrometer equipped with NMR teslameter (ER 036TM) and frequency counter (E 41 FC) at X- and Q-band. The experimental spectra were simulated using program Dublet (S=1/2) written by dr A. Ozarowski from NHMFL, University of Florida, with resonance field calculated by full diagonalization of the energy matrix.

The films were deposited by spin coating technique on Si(111) wafers (10\10 mm), glass and ITO. Precursors were dissolved in tetrahydrofuran and deposited on Si using a spin coater (Laurell 650SZ). The morphology and composition of the obtained layers were analyzed with a scanning electron microscope (SEM) LEO Electron Microscopy Ltd, England, model 1430 VP equipped with detectors of secondary electrons (SE), and energy dispersive X-ray spectrometer (EDS) Quantax with detector XFlash 4010 (Bruker AXS microanalysis GmbH). The atomic force microscopy AFM studies in the tapping mode were performed on Veeco (Digital Instrument) microscope Type: MultiMode NanoScope IIIa. The fluorescence spectra were recorded on a spectrofluorometer F-7000 HITACHI in the range 900-180 nm ($5x10^{-4}$ mol/dm^3 MeCN solution).

X-ray crystallography

The X-ray diffraction data of [Cu(II)(epy(di-*t*-Buba))Cl]x0.042H_2O (**1a**) and of [Cu(II)(epy(di-*t*-Buba))O_2CCH_3] (**1b**) were collected at room temperature using Oxford Sapphire CCD diffractometer, Mo Kα radiation λ = 0.71073Å. The reflections were measured with ω-2θ method and the analytical absorption correction was applied for the studied crystals (RED171 package of programs, Oxford Diffraction, 2000[31]). Both structures were solved by the direct methods and refined with full-matrix least-squares procedure on F^2 (package SHELX-97[32]). All heavy atoms were refined with anisotropic thermal displacement parameters. Hydrogen atoms were located from the electron density maps and their positions were constrained in the refinement. In (**1a**) the disordered water molecule is found on the C_{3i} axis and its total occupancy is 0.25. However, this molecule was unstable during the refinement and thermal parameter was high. Therefore we modelled the solvent disorder in SQUEEZY[33] and subsequently

the refinement in SHELXL-97 was repeated resulting in slightly better R factors and smooth diference electron density map. For (**1b**) the geometric restraints have been used to ensure the proper geometry of the disordered ^{t}Bu group. All figures were prepared in DIAMOND[34] and ORTEP-3[35]. The results of the data collections and refinement are listed in Table 1. The CCDC 950557 and 986880 entries contain the crystallographic data for (**1a**) and (**1b**), respectively. The details of the data can be obtained free of charge from The Cambridge Crystallographic Data Centre *via* www.ccdc.cam.ac.uk/data_request/cif.

Table 1. Crystal data and structure refinement for [Cu(II)(epy(di-*t*-Buba))Cl]x0.042H_2O (**1a**) and [Cu(II)(epy(di-*t*-Buba))O_2CCH_3] (**1b**).

Identification code	(**1a**)	(**1b**)
Empirical formula	$C_{22}H_{29.08}ClCuN_2O_{1.04}$	$C_{24}H_{32}CuN_2O_3$
Formula weight	437.21	460.06
Temperature [K]	293(2)	293(2)
Wavelength [Å]	0.71073	0.71073
Crystal system, space group	trigonal, R -3	monoclinic, $P2_1/c$
Unit cell dimensions [Å] and [°]	a = b = c = 15.8718(2) α= β= γ= 106.6390(10)	a = 17.296(2) b = 11.9783(9) c = 12.1930(11) β = 105.196(12)
Volume [Å^3]	3362.10(7)	2437.8(4)
Z, Calculated density [Mg·m^{-3}]	6, 1.296	4, 1.253
Absorption coefficient [mm^{-1}]	1.107	0.921
F(000)	1377	972
Crystal size [mm]	0.63 x 0.49 x 0.18	0.36 x 0.34 x 0.05
Theta range for data collection [°]	2.45 to 27.09	2.09 to 28.16
Limiting indices	-20<=h<=10 -20<=k<=20 -18<=l<=20	-21<=h<=20 -15<=k<=13 -10<=l<=16
Reflections collected/unique	22072 / 4873 [R(int) = 0.0839]	16433 / 5400 [R(int) = 0.0812]
Completeness to theta [%]	26.00º 99.9 %	25º 100.0 %
Max. and min. transmission	0.8256 and 0.5423	0.9577 and 0.7354
Data/restraints/parameters	4873 / 0 / 250	5400 / 0 / 298
Goodness-of-fit on F^2	0.9671.000	0.863
Final R Indices [I>2sigma(I)]	R1 = 0.0368, wR2 = 0.0956	R1 = 0.0527, wR2 = 0.1065
R indices (all data)	R1 = 0.0518, wR2 = 0.0990	R1 = 0.1424, wR2 = 0.1293
Largest diff. peak and hole [eÅ^{-3}]	0.364 and -0.228	0.549 and -0.518

Synthesis

Synthesis of ligands

Ligands (**1**-**4**) were prepared in a procedure described in details for (**1**) and their structural formula are presented at Figure 1.

pen(di-*t*-Buba) (**1**) Schiff base was prepared in reaction of 2-hydroxy-3,5-ditert-butyl-benzaldehyde (2.34 g; 10 mmol in 15 ml MeOH), with 2-(2-aminoethyl)pyridine) (1.19 ml; 10 mmol). The mixture was stirred at r. t. for 5h and solvent was removed on rotary evaporator. The product was dried on air. Yield 3.10 g (92.1%).

^{1}H [ppm]: 1.32 (s, 9H) CH_3, 1.46 (s, 9H) CH_3, 3.21 (t, 2H) CH_2-, 4.02 (t, 2H) CH_2, 7.045 (d 1H), 7.13-7.21 (m, 2H) Ar-H; 7.28 (s, 1H), 7.38 (d, 1H), 7.59-7.63 (m, 1H) Ar-H; 8.58-8.59 (m, 1H) Ar-H; 8.34 (s, 1H) -N=CH-; 13.76 (s, 1H)-OH.[36]

^{13}C [ppm]: 29.42 (C6), 31.5 (C7), 34.1 (C17), 35.03 (C18), 117.83 (C15), 121.47 (C2), 123.70 (C4), 125.83 (C14), 126.83 (C3), 136.43 (C11), 136.63 (C12), 139.93 (C13), 149.45 (C1), 158.10 (C5), 159.27 (C10), 166.39 (C8).

Uv-Vis 209 nm π→ π*, 261 nm π→ π*, 329 nm π→ $\pi^*_{N=C}$, 409 nm n→π*.[37-40]

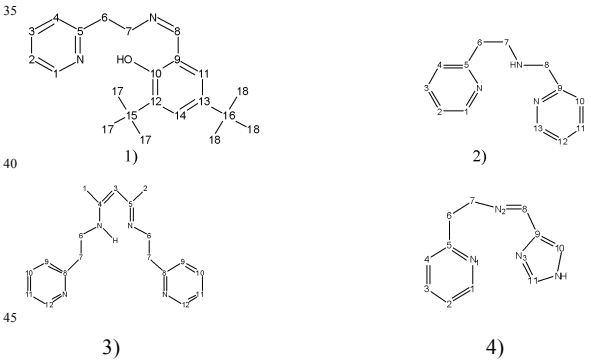

Figure 1 Structural formula and atoms numbering referring to the NMR signals for of epy(di-*t*-Buba) (**1**) (*Z*)-2,4-di-tert-butyl-6-((2-(pyridin-2-yl)ethylimino)methyl)phenol, epy(pyca) (**2**) 2-(4,5-dihydropyridin-2-yl)-*N*-(pyridin-2-ylmethyl)ethanamine, (epy)$_2$acacH (**3**) (2*Z*,4*E*)-*N*-(2-(pyridin-2-yl)ethyl)-4-(2-(pyridin-2-yl)ethylimino)pent-2-en-2-amine, epy(4Him) (**4**) (*E*)-*N*-((1*H*-imidazol-4-yl)methylene)-2-(pyridin-2-yl)ethanamine

epy(pyca) (**2**) ^{1}H [ppm]: 2.24 (s, 1H); 3.07 (m, 2H), 3.96 (s, 1H), 7.15 (m, 1H); 7.20 (d, 1H), 7.62 (m, 1H); 8.54 (m, 1H), 8.34 (s, 1H) -N=CH-;[36,41]

^{13}C [ppm]: 38.58 (C7), 49.01 (C6), 121.24 (C10), 121.88 (C2), 122.21 (C4), 123.29 (C12), 136.35 (C3), 136.43 (C11), 149.25 (C1), 149.31 (C13), 159.81 (C9), 160.21 (C5), 55.14 (C8).

^{15}N NMR [ppm]: -69.90 (-N=C), -342.47 (NH).

Uv-Vis: 211 nm π→ π*, 256 nm π→ π*, 324 nm π→ $\pi^*_{N=C}$, 400 nm n→π*.[37-40]

(epy)$_2$acacH (**3**) ^{1}H NMR [ppm]: 1.85 -CH_3 (s, 3H), 1.98 CH_3 (s, 3H), 3.04 (t, 4H) CH_2-Ar, 3.67 (q, 4H) CH_2-N, 4.92 (s, 1H) C=CH-C, 7.09-7.19 (4H), 7.62 (t, 2H) ArH, 8.55 (d, 2H) ArH, 10.90 (br s, 1H) NH-.[36]

^{13}C NMR [ppm]: 18.76 (C1) CH_3, 28.77 (C2) CH_3. 38.83 C(6), 42.73 C(7), 95.33 (C3), 121.75 (C11), 123.73 (C9), 136.60 (C10), 149.60 (C12), 158.25 (C8), 162.97 (C4), 194.86 (C5). Figure 1.

^{15}N NMR [ppm]: N(3) -N=C amine -266.3, -355.9 N(2) NH equals N(1) N=C, -68.7.[42]

Uv-Vis: 262 nm π→ π*, 307 nm π→ π*, 311 nm π→ $\pi^*_{N=C}$, 410 nm n→π*.[37-40]

The presence of signals at the ^{1}H, ^{13}C and ^{15}N spectra of (**3**) confirm the tautomeric structure of the isolated compound (**3**).[42-44]

epy(4Him) (**4**) ^{1}H NMR [ppm]: 3.11 (t, 2H) -CH_2-N=, 3.42 (s, 1H) -NH-, 3.92 (t, 2H) -CH_2-Ar, 7.08-8.48 (m, 6H) CH_{Ar}, 9.78 ppm (s, 1H) -N=CH-.[36]
^{13}C NMR [ppm]: 39.4 (C6), 60.5 (C7), 119.8 (C10), 121.6 (C2), 122.3 (C9), 123.7 (C4), 136.6 (C3), 137.7 (C11), 149.1 (C1), 152.6 (C8), 159.3 (C5).
Uv-Vis: 257 nm π→ π*, 341 nm π→ $\pi^*_{N=C}$, 406 nm n→π*.[37-40]

Synthesis of complexes

[Cu(II)(epy(di-*t*-Buba))Cl] (**1a**)
Copper(II) chloride dihydrate (1.70 g; 10mmol) in EtOH (10 ml) was added to an ethanolic solution (10 ml) of the ligand (**1**) (3.39 g; 10 mmol). The mixture was stirred for 4 h at r. t. Dark green crystals suitable for X-ray diffraction from C_2H_5OH/C_6H_6 were isolated. Yield: 3.600 g (79.3%), $C_{22}H_{29.08}ClCuN_2O_{1.04}$ (calc/found %): Cu 14.55/14.20, C 60.53/60.81, N 6.41/6.34, H 6.69/7.08.
Uv-Vis: 255 nm IL, 285 nm LMCT, 348 nm LMCT, 406 nm LMCT.[37-40]

[Cu(II)(epy(di-*t*-Buba))O_2CCH_3] (**1b**)
The compound was prepared in similar way as (**1a**) using copper(II) acetate hydrate (1.990 g, 10 mmol). Dark green single crystals of (**1b**) suitable for X-ray analysis were obtained from CH_3Cl/C_6H_6 solution. Yield: 3.340 g (72.7%). $C_{24}H_{32}CuN_2O_3$, calc/found %: Cu 13.81/13.55, C 62.65/62.30, N 6.08/6.23, H 7.01/6.78.
Uv-Vis: 238 nm LMCT, 308 nm LMCT, 390 nm LMCT.[37-40]

Complexes (**2a**), (**3a**), (**4a**) were synthetised in the way described above. Results of C, H, N analysis are as follows: [Cu(II)(epy(pyca))Cl_2] (**2a**) Yield: 80.6%. $C_{13}H_{13}CuN_3Cl_2$ calc/found %: Cu 18.38/18.27, C 45.36/45.71, N 12.15/12.11, H 3.79/3.99.
Uv-Vis: 202 nm IL, 260 nm IL, 309nm LMCT.[37-40]

[Cu(II)(($epy)_2$acacH))O_2CCH_3] (**3a**) Yield: 82.7%. $C_{21}H_{25}CuN_4O_2$ calc/found %: Cu 14.81/14.97, C 58.79/58.46, N 13.06/12.95, H 5.87/5.84.
Uv-Vis: 205 nm IL, 254 nm IL, 316 nm LMCT.[37-40]

[Cu(II)(epy(4Him))O_2CCH_3] (**4a**) Yield: 68.2%. $C_{13}H_{15}CuN_4O_2$ calc/found %: Cu 19.86/19.40, C 48.82/49.19, N 17.52/17.42, H 4.68/4.24.
Uv-Vis: 205 nm IL, 258 nm IL, 313 nm LMCT.[37-40]

Results and discussion

Structure of [Cu(II)(epy(di-*t*-Buba))Cl]x0.042H_2O (1a)

The [Cu(II)(epy(di-*t*-Buba))Cl]x0.042H_2O (**1a**) crystallized in the rhombohedral R-3 space group with the whole molecule in the asymmetric unit. However, the disordered and relatively poorly refined water molecule is excluded from the final model as it was mentioned in the Experimental part. The copper(II) coordination sphere is composed of two nitrogen atoms and one oxygen from the Schiff base and chloride (Figure 2). It adopts the strongly distorted square planar environment with angles in two ranges from 145.23(8) (O1-Cu1-N17) to 150.98(5) (N9-Cu1-Cl2) and from 93.12(7) (N9-Cu1-N17) to 96.03(5)° (N17-Cu1-Cl2). In the coordination sphere, the pyridine nitrogen occupies *cis* position relative to N9 and Cl atoms. O1 (phenol) atom is *trans* to N17 (pyridine) atom, whereas aliphatic N9 (azomethine) atom is *trans* to chloride. All Cu-X (X = N, O, Cl) bonds differ significantly with the shortest values observed for Cu-O1 (phenol) bond (1.8724(15) Å) and the biggest for Cu-Cl (2.2187(6) Å). The Cu-$N_{(aryl)}$ is much longer (by approximately 0.05 Å) than $N_{(alkyl)}$. The phenyl and pyridyl rings remain flat with r.m.s. of 0.006 Å. Two chelate rings differ significantly in their conformation: Cu1-O1-C2-C7-C8-N9 ring is flat with r.m.s. of 0.016 Å, whereas Cu1-N17-C12-C11-C10-N9 ring is strongly folded with r.m.s. of 0.296 Å and the largest deviation of 0.493(2) Å observed for C11.

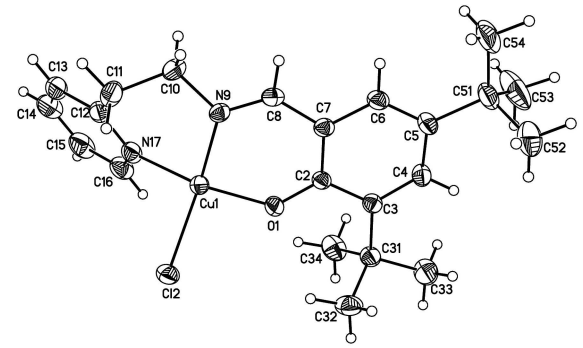

Figure 2 Molecule of [Cu(II)(epy(di-*t*-Buba))Cl]x0.042H_2O (**1a**) with the numbering scheme and thermal ellipsoids at 30% probability.

The phenyl and pyridine ring systems form a dihedral angle of 49.34(13)º. The phenyl and Cu1-O1-C2-C7-C8-N9 chelate ring are coplanar with an angle of 2.57(9)º, whereas Cu1-N17-C12-C11-C10-N9 chelate and pyridine rings are inclined by 27.54(12)º. Both chelate rings form an angle of 21.62(9)º. Hence, the Schiff base exhibits a bowl shape with copper(II) ion on its top and showing a shift by 0.51 Å from the plane defined by the coordinating O1, N9 and N17 atoms. Such orientation of aromatic rings is assured by conformation of the -CH=N-CH_2-CH_2- linker and the most important impact reveal dihedral angles around C10-C11 and C11-C12 bonds from the folded N17 chelate rings showing values of -62.1(3) and 61.4(3)º, respectively. The geometry of the Schiff base motif is described by C8-N9 distance of 1.283(3) and C7-C8-N9, C8-N9-C10 angles of being 128.03(19) and 115.66(17)º, respectively. The C2-C7-C8-C9 torsion angle describing geometry of the O1 chelate ring is -0.7(3)º indicating that this ring is flat as it was showed also by r.m.s. deviation.
The structure of (**1a**) reveals the porous nature with channels running along *c* axis filled with water molecules. Every channel is encompassed by six adjacent channels. They are surrounded by six complex molecules arranged in two inverted triangles forming …-AB-AB-... pattern of layers. The hyphen indicates large separation between triangles. It can be estimated as Cu-Cu

distance being 6.551 Å inside -AB- and 15.249 Å between B-A pairs of triangles. In the former case six molecules form a single pore. The diameter of these channels is approximately 5.2 Å. Hence, the water molecule located in this position could not interact with walls of the pore and should be easily removed. Therefore, it was unstable in the refinement and revealed high thermal parameter. Six molecules forming walls of the pore coming from -AB- layers are connected due to C10-H10…Cl2 (-z, 1-x, 1-y) hydrogen bonds. Additionally, there are numerous π-π interactions, mainly between strongly inclined rings of the molecules forming the pore and C15-H15…π interactions with O1 chelate ring. Interactions between adjacent -AB- modules in the channel, translated along *c* axis do not exist due to significant separations between molecules. However, there are interactions between adjacent modules from different channels. They concern two the closest copper(II) ions separated by 5.078 Å and are formed due to C11-H11…π interactions with phenyl ring and numerous π-π interactions, among them stacking interactions between close, well-oriented and revealing small slippage two O1 chelate rings.

Table 2. Selected interactions bond lengths [Å] and angles [°] for [Cu(II)(epy(di-*t*-Buba))Cl] (**1a**).

(**1a**)	Bonds		
Cu1-O1	1.8724(15)	Cu1-N17	1.9892(19)
Cu1-N9	1.9351(17)	Cu1-Cl2	2.2187(6)
	Angles		
O1-Cu1-N17	145.23(8)	N9-Cu1-Cl2	150.98(5)
N9-Cu1-N17	93.12(7)	N17-Cu1-Cl2	96.03(5)
O1-Cu1-N9	94.16(6)	O1-Cu1-Cl2	93.85(5)

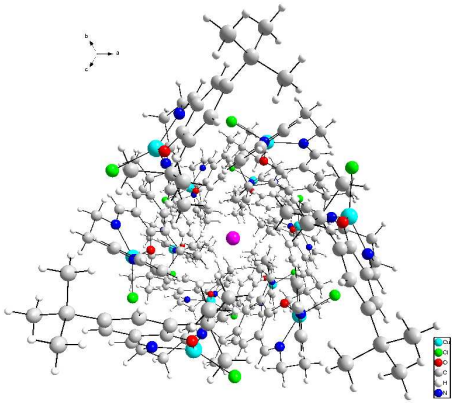

Figure 3 Perspective view of (**1a**) along [111] direction reveals channels of 5.2 Å diameter filled with partially occupied water molecules.

X-ray Crystal Structure of [Cu(II)(epy(di-*t*-Buba))O_2CCH_3] (1b)

In (**1b**) Cu(II) ion is coordinated by asymmetric Schiff base and acetate ligand (Figure 4) resulting in CuN_2O_3 square pyramidal geometry. Among the equatorial bonds, Cu1-O1(phenolate) distance of 1.878(3) Å is much shorter than that for Cu1-O2 (acetate) of 1.960(2) Å. There is a significant difference between Cu1-N1 (benzaldehyde) 1.937(3) and Cu1-N2 (pyridine) 1.989(3) Å, which is similar to that found in (**1a**). The axial bond Cu1-O3 of 2.517(3) Å is formed by the acetate oxygen. Different C23-O bond lengths for the carboxylate anion (Table 3) were noted, indicating that O2 is a carboxylate atom, while O3 forms a double bond to C23.

The CuN_2O_2 equatorial plane exhibits a significant tetrahedral deformation with the atom displacement from the best plane ranging from O1 0.440(2) Å to O2 -0.399(1) Å. Atoms N1 and O2 are displaced from the CuN_2O_2 plane towards axial O3, while O1 and N2 are displaced in an opposite direction. Similar geometry of the square-planar coordination sphere was reported for [{(2-etpy)(sal))Cu}{μ-[$Ag(CN)_2$]}] and [{(2-etpy(sal))Cu}{μ-[$Cu(CN)_2$]}] complexes.[45] In the equatorial plane, the pairs of atoms positioned *trans* define N1-Cu1-O2 and O1-Cu1-N2 angles of 159.90(11) and 151.58(11)º, respectively, the values larger than those reported for (**1a**). The angles formed by the atoms in the *cis* positions range from 90.10(11) to 94.87(14) and are significantly smaller that those found in (**1a**). That seems to reflect the difference caused by the bulk of chloride ligand in (**1a**). The angles between equatorial bonds formed by O1, N1 and N2 and axial Cu1-O3 are 97.44(11), 103.36(10) and 107.25(10)º, respectively. The O2-Cu1-O3 angle involving both oxygen atoms of the acetate ligand equals 56.54(9)º.

The dihedral angle between the phenolate and pyridyl rings of the Schiff base ligand is 13.6(2)º and is much smaller than that reported for (**1a**). Such a flat environment may be coupled to the position of the acetate ligand, almost perpendicular to the plane defined by both these rings, with the dihedral angles between phenolate and pyridyl rings and the plane Cu1-O2-C23-O3 being 79.46(12) and 76.54(10)º, respectively. The torsion angle Cu1-O2-C23-O3 describing the rotation of acetate around the coordination Cu1-O2 bond is 8.2(5)º. The acetate ligand is slightly tilted relative to the equatorial CuN_2O_2 plane, with the dihedral angle between these planes being 80.41(15)º.

Table 3. Selected bond lengths [Å] and angles [º] for [Cu(II)(epy(di-*t*-Buba))O_2CCH_3] (**1b**).

Cu1-O1	1.878(3)
Cu1-N1	1.937(3)
Cu1-O2	1.960(2)
Cu1-N2	1.989(3)
Cu1-O3	2.517(3)
O1-Cu1-N1	92.84(13)
O1-Cu1-O2	90.10(11)
N1-Cu1-O2	159.90(11)
O1-Cu1-N2	151.58(11)
N1-Cu1-N2	94.87(14)
O2-Cu1-N2	91.92(11)
O3-Cu1-O1	97.44(11)
O3-Cu1-O2	56.54(9)
O3-Cu1-N1	103.36(10)
O3-Cu1-N2	107.25(10)
C1-O1-Cu1	126.5(2)
C7-N1-Cu1	121.9(3)
C8-N1-Cu1	119.8(3)
C10-N2-Cu1	122.8(3)
C14-N2-Cu1	118.6(3)
C23-O2-Cu1	102.7(2)

The valence geometry of the Schiff base ligands is typical for such systems. The C7-N1 distance is 1.280(5) Å, C6-C7-N1 and C7-N1-C8 angles are 127.0(4) and 117.8(3)º, respectively and are similar to those observed in (**1a**). The phenolate-Schiff base moiety of the ligand is almost flat, with the torsion angles C1-C6-C7-N1 and C6-C7-N1-C8 being 8.9(6)º and -178.0(3)º. However, ethylaminepyridil fragment is significantly folded with

consecutive torsion angles C7-N1-C8-C9, N1-C8-C9-C10 and C8-C9-C10-N2 being -140.6(3), -72.8(5) and 54.9(5)º. The C19 ^{t}Bu group reveals a rotational disorder with two equally populated rotamers (50/50%).

The six-membered chelate rings Cu1-O1-C1-C6-C7-N1 and Cu1-N1-C8-C9-C10-N2 are an envelope on Cu1 and a boat, respectively. In the four-membered ring Cu1-O2-C23-O3 the torsion angles have alternating negative and positive values ranging from -6.4(4) to 8.2(5)º.

Analysis of crystal packing revealed the π-π interaction between C1-C6 phenyl ring and pyridine C10-N2[1-x,-y,-z] with the angle between two rings 13.57º and distance between their gravity centers Cg-Cg of 3.885(3) Å. There is an intermolecular C7-H7A...O3[x,-1/2-y,-1/2+z] interaction involving the Schiff base C-H and acetate oxygen, with C…O distance of 3.398(4) Å (Figure 5). Two methyl groups of C15 ^{t}Bu are involved in the intramolecular interactions C16-H16C...O1 and C17-H17B...O1, with C…O distances being 2.958(6) and 2.958(7) Å, respectively.

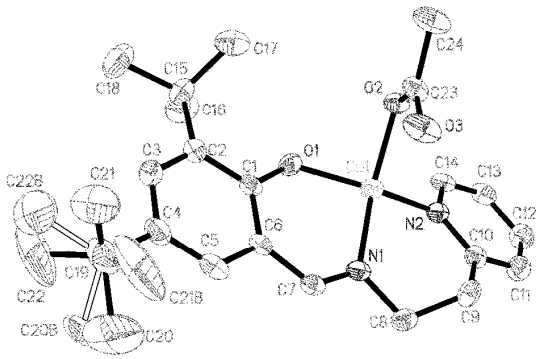

Figure 4 Molecule of [Cu(II)(epy(di-*t*-Buba))O_2CCH_3] (**1b**) with the numbering scheme and thermal ellipsoids at 30% probability. For clarity H atoms for the disordered ^{t}Bu were omitted.

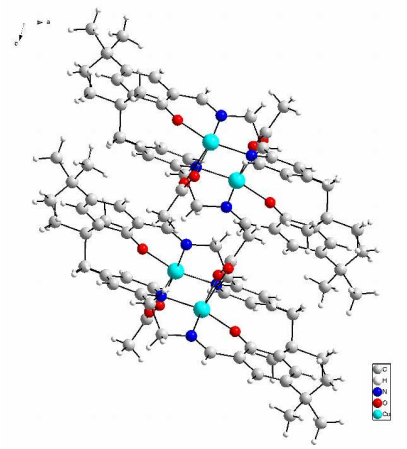

Figure 5 Packing of (**1b**) viewed along *c* axis.

Both reported structures have different counterions, that heavily influence the packing and absorption properties. Only (**1a**) structure is porous (Figure 3). Moreover, at the molecular level the counterions affect the coordination number. In (**1a**) the coordination sphere adopts strongly distorted square planar environment, whereas in (**1b**) it is strongly elongated tetragonal pyramid. In both cases the valence geometry of the Schiff base is similar. However, some conformational differences are detected, of which the most important occurs for C8-N9-C10-C11 angle, being -171.98(19)º in (**1a**) and -140.6(3)º in (**1b**) structure.

EPR analysis

The EPR spectra at Q–band of polycrystalline compounds [Cu(II)(epy(di-*t*-Buba))Cl] (**1a**) and [Cu(II)(epy(di-*t*-Buba))O_2CCH_3] (**1b**) exhibit much better resolution of two signals for (**1a**) and three signals for (**1b**) (Table 4) than those measured at X-band, (Figure 6). Although the EPR spectra could be treated as showing an axial and orthorhombic symmetry of the Cu(II) centers, respectively, the values of g_1 parameters are too small considering: a) a type of donors coordinated in Cu(II) plane, (NON)Cl and (NON)O, and b) a significant deviation of planar to tetrahedral geometry, which imposes the increase of g-matrix diagonal components.[46]

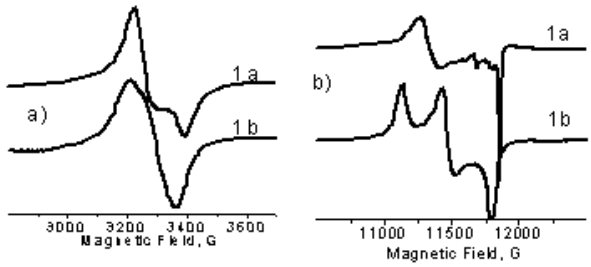

Figure 6. EPR of polycrystalline compounds (**1a**) and (**1b**) a) at X-band (about 9.7 GHz) at room temperature and b) at Q-band (about 36 GHz) at room temperature. The weak signals for (**1b**) in the middle of spectrum at Q-band corresponds to the resonance transitions due to differently oriented crystallites

Hence, the spectra can be considered as a result of cooperative effects due to the magnetic exchange between the non equivalent paramagnetic centers. The observed values of the g components are caused by the coupling of g matrixes giving g_1^c, g_2^c and g_3^c parameters (Table 4). The crystal structure reveals that for [Cu(II)(epy(di-*t*-Buba))Cl] (**1a**) the interactions may arise at the shortest Cu…Cu distance of 6.550 Å, for non-parallel coordination polyhedra, which planes Cl2 O1 N17 N9 are canted by 60.41º. The monomeric units are joined by C10-H10…Cl2 interactions and numerous π-π interactions, mainly between strongly inclined rings of the molecules. For [Cu(II)(epy(di-*t*-Buba))O_2CCH_3] (**1b**) the dihedral angle between Cu1-O2-O1-N1-N2 planes is 76.23º for the Cu(II) centers separated by 6.352 Å. There are also intermolecular C7-H7A...O3 interactions involving the Schiff base C-H and acetate oxygen as well as π-π interactions between inclined phenyl and pyridine rings.

The Q-band spectra of [Cu(II)(epy(di-*t*-Buba))Cl] (**1a**) and [Cu(II)(epy(di-*t*-Buba))O_2CCH_3] (**1b**) are similar to those reported[47-48] for Cu(II) complexes with tridentate ONO Schiff bases and monodentate X ligands, Cu(salgly)diPhTuxH$_2$O where salgly = N-salicylidene-glycine and diPhTu =*N*,*N*'-diphenylthiourea and Cu(salval)P x P where salval= *N*-salicylidene-(*R*,*S*)-valine, P=pyrazole. The molecular EPR parameters were calculated for those complexes using the approximate relations between the canting angles (the angles formed by the tetragonal axis of magnetically non-equivalent

chromophores)[47] and the coupled g_c components. Although the coupled g components listed in Table 4 have very close values, the molecular g tensor components of individual [Cu(II)(epy(di-*t*-Buba))Cl] (**1a**) and [Cu(II)(epy(di-*t*-Buba))O_2CCH_3] (**1b**) complexes should exhibit stronger rhombicity than the parameters calculated for Cu(II) complexes with ONO Schiff bases. The latter can be caused by significant tetrahedral distortion in Cu(II) plane in [Cu(II)(epy(di-*t*-Buba))Cl] (**1a**) and [Cu(II)(epy(di-*t*-Buba))O_2CCH_3] (**1b**). Also a higher value of g_z should be expected, close to 2.26 according to the parameters observed for Cu(II) complexes with different tridentate ONN[49] and ONN[50] Schiff bases and polar solvents.

Table 4. EPR spectra of coupled and molecular g matrix parameters and crystal structure data for (**1a**) and (**1b**)

			c	g_{av}	Cu - Cu [Å]	canting angle [°]	
Cu(salgly)diPhTu xH_2O	g_1^c=2.145	g_2^c=2.145	g_3^c=2.042	2.111		90*	47
	g_z=2.228*	g_y=~2.065	g_x=~2.04*	2.111			
Cu(salval)P x P	g_1^c=2.179	g_2^c 2.127	g_3^c=2.050	2.119	6.131	74.0	48
	g_z=2.247*	g_y=2.066*	g_x=2.045*	2.119			
[Cu(II)(epy(di-*t*-Buba))Cl] (**1a**)	g_1^c=2.146	g_2^c=2.146	g_3^c=2.047	2.113	6.550	60.41	This s
[Cu(II)(epy(di-*t*-Buba))O_2CCH_3] (**1b**)	g_1^c=2.180	g_2^c=2.115	g_3=2.059	2.118	6.352	76.23	This s

*calculated on the basis of EPR data

Infrared spectroscopy

The IR spectra of free ligands exhibit bands from -N=CH- stretching vibrations in the region 1591-1623 cm^{-1}.[37,54] Spectrum of epy(di-*t*-BubaH) (**1**) exhibits the Ph-O stretching vibrations band at 1235 cm^{-1}, whereas -OH stretching vibrations band was noted at 3467 cm^{-1}. Upon complexation, Ph-O stretching vibrations band was shifted towards higher frequencies (1256 cm^{-1} for (**1a**) and 1251 cm^{-1} for (**1b**)), while -OH stretching vibrations bands have disappeared.[51-53]

Moreover, the band from azomethine stretching vibrations in (**2a**) was noted at 1608 cm^{-1} for [Cu(II)(epy(pyca))Cl_2], $\Delta_{coord}= \Delta_{comp}-\Delta_{lig}$=17 cm^{-1} for (**2a**), what confirms the copper binding by -N=CH- group. Also, the stretching vibrations of -NH- for (**2a**) were observed at 3446 cm^{-1} (Δ=12 cm^{-1}) for (**2a**), what confirms the coordination *via* pyridine nitrogen atom. In the spectrum of [Cu(epy(di-*t*-Buba))Cl]x0.042H_2O (**1a**) at 3436 cm^{-1} a band from stretching vibrations of the -OH group was registered.

In the spectra of [Cu(II)(epy(4Him))O_2CCH_3] (**4a**), (**1b**) and [Cu(II)((epy)$_2$acacH)O_2CCH_3)] (**3a**) the bands from symmetrical and asymmetrical stretching vibrations of the carboxylate group in the region 1403-1474 cm^{-1} ν_sCOO^- and 1628-1742 cm^{-1} $\nu_{as}COO^-$ were registered[54], suggesting the monodentate coordination.

Moreover, the band from Cu-N vibrations was noted at 428 cm^{-1} (**2a**), whereas the band from Cu-O stretching vibrations was registered at 507cm^{-1} (**4a**), at 543 cm^{-1} (**1a**), at 588 cm^{-1} (**1b**), and 526 cm^{-1} (**3a**).[55] Additionally, band from Cu-Cl stretching vibrations appears at: 309 cm^{-1} [Cu(II)(epy(pyca))Cl_2] (**2a**) and 352 cm^{-1} (**1a**).[54] The presence of the bands from Cu-O, Cu-N and Cu-Cl stretching vibrations confirm the coordination *via*: Ph-O, N and Cl atom respectively.

Summarizing IR results for the studied complexes it is evident, that the copper(II) ions coordinate with ligand *via* N or O atoms and Cl^- or CH_3COO^- ions.

Thermal analysis of the complexes

DTA curve of [Cu(epy(di-*t*-Buba))Cl] (**1a**) revealed endothermic process between 38 – 998 °C. Analysis of the DTG curve indicates one process corresponding to the detachment of the organic ligand (TG mass loss 71.24%). The final product of decomposition was CuCl (calc. 16.83%, exp. 16.34%) what was confirmed by the XRD analysis.

The decomposition of [Cu(II)(epy(di-*t*-Buba))O_2CCH_3] (**1b**) is also the one step endothermic process (Figure 7). On DTG peak (T_{max} =266 °C, 77.85% sample mass loss) corresponds to the Schiff base detachment was observed. The final product of decomposition was the mixture of CuO with carbon impurities.

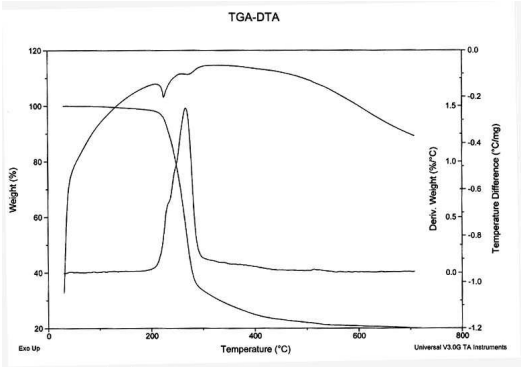

Figure 7. Thermogram of [Cu(II)(epy(di-*t*-Buba))O_2CCH_3] (**1b**).

The thermal decomposition of the [Cu(II)((epy)$_2$acacH))O_2CCH_3] (**3a**) is an exothermic process (T_i=145 °C, T_{max}=191 °C and T_f=1190 °C). As for (**1a**) and (**1b**), the final product of decomposition was CuO (mass of residue calc. 18.94%; exp. 18.32%).

In case of [Cu(II)(epy(pyca))Cl_2] (**2a**) the decomposition is the multi stage process (T_i = 26 ºC and T_f=964 ºC). On the DTG curve seven exothermic processes with maxima at: 58 ºC, 163 ºC, 17 5ºC, 249 ºC, 329 ºC, 437 ºC and 1010 ºC were observed, which can be assigned to the detachment of chlorine and partial decomposition of the Schiff base (total mass loss 81.40%). The final product of decomposition process was metallic Cu (calc. 18.6 %, exp. 18.6%).

Thermogram of [Cu(II)(epy(4Him))O_2CCH_3] (**4a**) exhibits four DTG peaks with maxima at 314, 394, 505 and 642 ºC, and TG curve reveals four stages with 3.68, 7.75, 29.27 and 11.30% sample mass loss. The first step with maximum at 184 °C at the DTA curve can be related to the detachment of the acetic acid molecule (mass loss 18.66%, calc. 18.69%). The assignment was confirmed by the IR spectra of gases evolved during measurement, where the bands at 1394 and 1774 cm^{-1} from ν_{COO^-}

$_{sym}$ and $\nu_{COO-\ asym}$ vibrations were observed.[39] Afterwards the partial dissociation of the Schiff base occurs leaving the metallic copper (the % mass residue 17.42% calc., exp. 19.78%). In the studied cases, the final product of the thermal decomposition of copper(II) complexes was copper oxide or metallic copper. The [Cu(II)(epy(4imH))O_2CCH_3] (**4a**) complex is thermally more stable than others because it was not completely decomposed below 1200 °C.

Thin layer studies

The copper(II) organic-inorganic layers on a silicon substrate were deposited by the spin coating technique. Because parameters of the layers depended on the spin speed, and time of coating for all experiments time was set to 30 s and spin speed 900, 1000, 1100 and 2000 rpm. The layers morphology were studied by SEM/EDX.

The SEM images revealed that silicon surfaces are uniformly covered by the Cu(II) complex. The layers are amorphous, but sporadically a crystalline structures appeared. The calculated dimensions of these crystallites ranged from 0.5 to 2.0 μm. The latter can be caused by non-completed solidification of the complex solution during the spin coating process. The EDS results indicated the copper contents decrease in the layers obtained at higher rotation speed. The latter corresponds to a thinner layer formation upon the increase of the rotation speed. For majority complexes, the best coverage and smooth layers were obtained at 1100 rpm and time 30 s. The obtained surfaces, in particular their roughness and thickness, were analyzed by AFM measurements and results are presented at Figure 8.

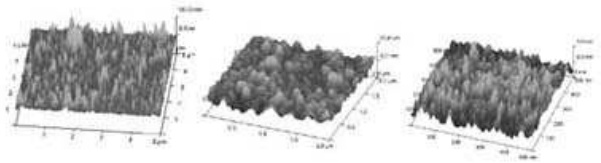

Figure 8. AFM images of the [Cu(II)(epy(pyca))Cl_2] (**2a**)/Si(111) layers: a) 900 rpm/min, b) (**2a**)/glass 1000 rpm/min, c) (**2a**)/ITO 1000 rpm/min

The images on Figure 8 reveal that the smallest and most uniform particles are on Si surface, whereas on ITO there are highest dimensions of the complex particle. On the glass substrate, particles revealed the biggest dissipation of variation in size and did not cover the substrate surface uniformly. Complex [Cu(II)(epy(pyca))Cl_2] (**2a**) forms layers uniformly covering the silicon surfaces at all used spin speeds. Deposition of compound (**2a**) on the glass slides and ITO was also performed (Figure 8). The highest value of R_q and R_a (average of image data without application of the surface height deviations measured from the mean plane) parameters were registered for the layers covering the glass slides. These measurements indicated that type of the substrate also affects the morphology of the obtained layer. In the case of (**2a**) the layers deposited on glass are rougher then those obtained on silicon or on ITO substrates. The uniformly covered materials were received at 900, 1000, 2000 rpm/min spin speed.

In the case of (**1a**)/Si and [Cu(II)(epy(di-*t*-Buba))O_2CCH_3] (**1b**)/Si, the homogenous layers without significant differences in roughness were obtained. The optimal spin speed was 1100 rpm/min, (R_q and R_a parameters equal 35.1 and 24.9 nm for (**1a**)/Si and 103 and 70.1 nm for (**1b**)/Si). For (**1a**)/Si, doubling of the spin speed and repetition of this process (time 10 s) leads to the smoother layer with: R_q=0.572 nm and R_a=0.842 nm. The depth of the layer equals 6 nm. For (**4a**)/Si, the optimal spin speed giving the smooth layer with equally spread compound was 2000 rpm/min (R_a =15.3 nm). The contents of Cu in this layer equals 3.11%.

The above discussion suggest that quality of the layer (uniformity, roughness) can be optimized by variation of spin speed and deposition time. Concluding, the obtained layers are thin, homogenous with equally spreaded complexes over the substrate surface.

Fluorescence properties of the layers

The Schiff bases are known for their fluorescence properties and their varied applications.[56-57] Therefore, we studied the luminescence properties of the obtained compounds and layers.

In the case of (**1a**) and (**1b**), the highest fluorescence bands intensity were observed for λ_{ex}=269 nm and 280 nm for [Cu(II)(epy(di-*t*-Buba))Cl] (**1a**) and [Cu(II)(epy(di-*t*-Buba))O_2CCH_3] (**1b**) respectively. The emission band from intraligand π*→π transitions was observed at 538 nm for (**1a**) and 560 nm for (**1b**).[37-39] The highest fluorescence intensity of the layer (**1a**)/Si and (**1b**)/Si was noted when rotation speed was set to 2000 rpm/min. These layers revealed the best smooth and uniformity. Besides that EDX results indicated that these layers exhibited the highest content of copper (12.48% for (**1a**) and 6.84% for (**1b**)).

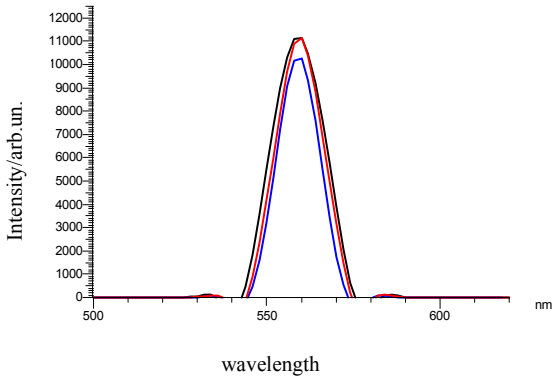

Figure 9. Fluorescence spectra of [Cu(II)(epy(pyca))Cl_2] (**2a**)/Si, ---- 900 rpm/min, - - - 1000rpm/min, - - - 1100 rpm/min, λex=280 nm, λem=560 nm.

The [Cu(II)(epy(4Him))O_2CCH_3] (**4a**)/Si, [Cu(II)((epy)$_2$acacH)O_2CCH_3] (**3a**)/Si materials also exhibit fluorescence λ_{em}=552 and 588 nm, (λ_{ex}= 277 (**4a**)/Si and 295 nm (**3a**)/Si). These layers were obtained at 1100 rpm/min (R_a=19.7 nm (**4a**)), respectively. Again they revealed the highest contents of the copper.

When the spin speed was set to 2000 rpm/min, the highest intensity of the fluorescence (λ_{em}=560 nm) was observed for (**2a**)/Si material (λ_{ex}=280 nm) (Figure 9). However, the hybrid layers of (**2a**) on the glass slides exhibit lower intensity then on the silicon wafers. The optimal spin speed for (**2a**)/ITO was 1000 rpm/min when the excitation was set at 250 nm and λ_{em}= 498 nm. Additionally, the copper(II) complexes fluorescence spectra were also recorded in MeCN solution. The spectra exhibited emission

bands between 365 and 588 nm from intraligand π*→π transition, (λ_{ex} = 277-295 nm). Spectra of complexes registered in solution revealed much lower intensity of the fluorescence bands than the bands of complexes layers.

These studies suggest, that better smoothnest of layers and higher complex concentration results in higher fluorescence intensity.

Conclusions

The series of the Schiff bases and their copper(II) complexes were obtained. The X-ray crystal data for copper(II) complexes indicated the planar environment strongly distorted towards tetrahedron geometry in the case of the [Cu(II)(epy(di-*t*-Buba))Cl]x0.042H_2O (**1a**). This structure reveals porous nature with channels filled with water molecules running along *c* axis. In complex [Cu(II)(epy(di-*t*-Buba))O_2CCH_3] (**1b**) Cu(II) ion is coordinated in CuN_2O_3 square pyramidal geometry by Schiff base and acetate ligands. The X-ray analysis results suggested the significant influence of the anion on the geometry of the coordination sphere. The EPR studies revealed the cooperative effects due to magnetic interactions between Cu(II) ions forming non-parallel coordination polyhedra. The final products of the thermal decomposition were either copper oxide or metallic copper and even a mixture of the copper oxide with carbon. The thin layers containing copper(II) Schiff bases complex exhibited fluorescence. The highest intensity of the fluorescence was noted for the smooth layers obtained at 1100 rpm/min or 2000 rpm/min which revealing the highest copper content. The emission was observed at 490-560 nm and is connected to the intraligand π*→π transitions. The fluorescence emission of the layers make these materials potentially suitable for application in light emitting devices.

Acknowledgements

Authors would like to thank the National Science Centre (NCN) Poland for financial support (grant no. 2013/09/B/ST5/03509).

References

(1) L. N. Wang, W.W. Qin and W. S. Liu, *Inorg. Chem. Commun*., 2010, **13**, 1122-1125.
(2) P. A. Vigato, S. Tamburini and L. Bertolo, *Coord. Chem. Rev*., 2007, **251**, 1311-1492.
(3) M. Shavit and E. Y. Tshuva, *Eur. J. Inorg. Chem*., 2008, 1467-1474.
(4) M. Zhao, B. Helms, E. Slonkina, S. Friedle, D. Lee, J. DuBois, B. Hedman, K. O. Hodgson, J. M. J. Frechet and S. J. Lippard, *J. Am. Chem. Soc*., 2008, **130**, 4352-4363.
(5) L. Dubois, J. Pecaut, M.-F. Charlot, C. Baffert, M.-N. Collomb, A. Deronzier and J.-M. Latour, *Chem. A Eur. J*., 2008, **14**, 3013-3025.
(6) C. I. Yang, W. Wernsdorfer, Y.-J. Tsai, G. Chung, T.-S. Kuo, G.-H. Lee, M. Shieh and H.-L. Tsai, *Inorg. Chem*., 2008, **47**, 1925-1939.
(7) M. Vasconcellos-Dias, C. D. Nunes, P. D. Vaz, P. Ferreira and M. J. Calhorda, *Eur. J. Inorg. Chem*., 2007, 2917-2925.
(8) S. Jong-Keun, Z. Long-Xuan, B. Arjun, T. Pritam, K. Radha, N. Younghwa, J. Yurngdong, J. Tae Cheon, J. Byeong-Seon, L. Chong-Soon and L. Eung-Seok, *Eur. J. Med. Chem*., 2008, **43**, 675-682.
(9) P. Kumar, S. Gorai, M. Kumar Santra, B. Mondal and D. Manna, *Dalton Trans*., 2012, **41**, 7573-7581.
(10) W. A. Alves, G. Cerchiaro, A. Paduan-Filho, D. M. Tomazela, M. N. Eberlin and A. M. Da Costa Ferreira, *Inorg. Chim. Acta*, 2005, **358**, 3581-3591.
(11) M. Mimura, T. Matsuo, T. Nakashima and N. Matsumoto, *Inorg. Chem*. 1998, **37**, 3553-3560.
(12) Y. Sunatsuki, Y. Motoda and N. Matsumoto, *Coord. Chem. Rev*., 2002, **226**, 199-209.
(13) M. Szybowicz, T. Runka, M. Drozdowski, W. Bała, A. Grodzicki, P. Piszczek and A. Bratkowski, *J. Mol. Struc*., 2004, **704**, 107-113.
(14) S. Park, J. S. Seo and S. Y. Park, *Adv. Funct. Mater*. 2012, **14**, 8878-8884.
(15) C. H. Chen and J. Shi, *Coord. Chem. Rev*., 1998, **171**, 161–174.
(16) C. Sanchez, L. Rozes, F. Ribot, C. Laberty-Robert, D. Grosso, C. Sassoye, C. Boissiere and L. Nicole, *C. R. Chim*., 2010, **13**, 3–39.
(17) B. Brauer, D. R.,T. Zahn, T. Ruffer and G. Salvan, *Chem. Physics Lett*., 2006, **432**, 226-229.
(18) C. M. Che, S. C. Chan, H. F. Xiang, M. C. W. Chan, Y. Liu and Y. Wang, *Chem. Commun*., 2004, 1484–1485.
(19) T. Sano,Y. Nishio,Y. Hamada, H. Takahashi, T. Usuki and K. Shibata, *J. Mater. Chem*., 2000, **10**, 157–161.
(20) K. H. Chang, C. C. Huang, Y. H. Liu, Y. H. Hu, P. T. Chou and Y. C. Lin, *J. Chem,. Soc. Dalton Trans*., 2004, 1731–1738.
(21) R. Ghosh, Sk. H. Rahaman, Chun-Nan Lin, Tian-Huey Lu and B. K. Ghosh, *Polyhedron*, 2006, **25**(16), 3104–3112.
(22) Yunbin Hu, Xike Gao, Chong-an-Di,Xiao di Yang, Feng Zhang, Yunqi Liu, Hongxiang Li and Daoben Zhu, *Chem.Mater.*, 2011, **23**(5), 1204–1215.
(23) Sanghyuk Park, Jangwon Seo, Se Hun Kim, and Soo Young Park, *Adv. Funct. Mater*. 2008, **18**, 726–731.
(24) I. Sorar, M. K. Şener, F. Z. Tepehan, A. Gül and M. B. Koçak, *Thin Solid Films*, 2008, **516**, 2894-2898.
(25) W. Ting-ting, He Zhi-qun, Z. Xiao-pan, W. Yong-sheng, Z. Chun-xiu and Z. Wen-guan, *Optoelectronics Letters*, 2007, **3(1)**, 43-46.
(26) W. Qiu, W.Hu, Y. Liu, S. Zhou, Yu Xu and D. Zhou, *Sensors & Actuators*, 2001, **B 75**, 62-66.
(27) P. M. Sirimanne, M. Rusop, T. Shirata, T. Soga and T. Jimbo, *Mat. Chem. and Phys*., 2003, **80**, 461-465.
(28) A. Jakob,T. Rüffer, P. Djiele, P. Ecorchard, B. Walfort, K. Körbitz, S. Frühauf, S. E. Schulz, T. Gessner and H. Lang, *Z. Anorg. Allg. Chem.* 2010, **636**, 1931–1940.
(29) M. Barwiolek, E. Szlyk, J. Lis and T Muziol, *Dalton Trans*., 2011, **40(41)**, 11012-11022.
(30) M. Barwiolek, E. Szlyk, A. Surdykowski and A. Wojtczak, *Dalton Trans*., 2013, **42**, 11476-11487.
(31) CrysAlis RED and CrysAlis CCD. Oxford Diffraction Ltd., Abingdon, Oxfordshire, England, 2000.
(32) G. M. Sheldrick, *Acta Crystallogr*., Sect. A, 2008, **64**, 112.
(33) A. L. Spek, Platon package, *Acta Cryst*. 2009, D65, 148-155.
(34) K. Brandenburg, DIAMOND, Release 2.1e. Crystal Impact GbR, Bonn, Germany, 2001.
(35) L. J. Farrugia, *J. Appl. Crystallogr*., 1997, **30**, 565.
(36) H. Günther, *NMR Spectroscopy, Basic Principles, Concepts, and Applications in Chemistry*, Wiley &Sons, 1995.
(37) M. Gullotti, A. Pasini, P. Fantucci, R. Ugo and R. D. Gillard, *Gazz. Chim. Ital*., 1972, **102**, 855-892.
(38) R. C. Felicio, G. A. da Silva, L. F. Ceridorio and E. R. Dokal, *Synth. React. Met. Org. Chem.*, 1999, **29**(2), 171-192.
(39) H. E. Smith, J. R. Neergaard, E. P. Burrows and F.-M. Chen, *J. Am. Chem. Soc*., 1974, **96**(9), 2908-2916.
(40) A. B. P. Lever, *Inorganic Electronic Spectroscopy*, Hoboken, NJ, Wiley-Interscience, 2006.
(41) M. Shakir, M. Azam, Y. Azim, S. Parveen and A. U. Khan, *Polyhedron*, 2007, **26**, 5513-5518.
(42) W. Schlif, B. Kamieński and T. Dziembowska; *J. Mol. Struct*., 2002, **602-603**, 41-47.
(43) P. T. Kaye and K. W. Wellington, *Synth. Commun*., 2001, **31**(16), 2405-2411.
(44) J. A. Connor and R. J. Kennedy, *J. Chem. Soc. Perkin Trans*., 1990, **2**, 203-207.
(45) C. Maxim, F. Tuna, A. M. Madalan, N. Avarvari and M. Andruh, *Cryst. Growth Des*. 2012, **12**, 1654-1665.
(46) Ch. M. Wansapura , Ch. Juyoung, J. L. Simpson, D. Szymanski, G. R. Eaton, S. S. Eaton and S. Fox, *J. Coord. Chem*., 2003, **56**, 975-993.
(47) G. Plesch, C. Friebel, O. Švajlenová and J. Krätsmár-Šmogrovič , *Polyhedron*, 1995, **14**, 1185-1193.
(48) G. Plesch, C. Friebel, S. A. Warda, J. Sivy and O. Švajlenová, *Transition Met. Chem*., 1997, **22**, 433-440.

(49) J. Jezierska, A. Jezierski, B. Jezowska-Trzebiatowska and A. Ozarowski, *Inorg. Chim. Acta*, 1983, **68**, 7-13.
(50) M. Leluk, B. Jezowska-Trzebiatowska and J. Jezierska, *Polyhedron*, 1991, **10**, 1653-1656.
(51) M. Asadi, B. Hemmateenejad and M. Mohammadikish; *J. Coord. Chem.*, 2010, **63**, 124-135.
(52) P. Zabierowski, J. Szklarzewicz, K. Kurpiewska and K. Lewiński, *Polyhedron*, 2013, **49**, 74-83.
(53) K. Nakamoto, *Infrared and Raman Spectra of Inorganic and Coordination Compounds*, Wiley, New York, 2009.
(54) P. Gluvchinsky and G. M. Mockler, *Spectrochim. Acta*, Part A, 1997, **33**, 1073-1077.
(55) E. Hadjoudis, A. Rontoyianni, K. Ambroziak, T. Dziembowska and I. M. Mavridis, *J. Photochem. Photobiol.*, A, 2004, **162**, 521-530.
(56) A. Mukherjee, A. Dutta, A. D. Jana and G. K. Patra, *Inorg. Chim. Acta*, 2013, **404**, 131-143.

Notes and references

[a]Chemistry Department, Nicholas Copernicus University, 87-100 Torun, Poland. Fax: +48 (56) 654 24 77; Tel: + 48 (56) 611 45 16, e-mail: madzia@chem.umk.pl, mbarwiolek@umk.pl,
[b]Faculty of Chemistry, University of Wroclaw, 50-137 Wroclaw, Poland, Fax: +48 71 328-23-48; Tel: +48 (71)3757330, e-mail: julia.jezierska@chem.uni.wroc.pl,